Diyala Journal of Engineering Sciences

Journal homepage: https://djes.info/index.php/djes

ISSN: 1999-8716 (Print); 2616-6909 (Online)

Optimization of PI Controller for a Photovoltaic Virtual Synchronous Generator System with Whale Optimization Algorithm

Mohanad Abd Shehab*

Electrical Engineering Department, College of Engineering, Mustansiriyah University, Baghdad, Iraq

ARTICLE INFO

Article history:
Received:28/06/2025.
Revised: 14/01/2026.
Accepted: 01/04/2026.
Available online: 15/06/2026.

Keywords:
Photovoltaic (PV)
Renewable Energy Sources (RES)
Virtual Synchronous Generator (VSG)
Whale Optimization Algorithm (WOA)
Proportional-Integral (PI) controllers

ABSTRACT

Traditional power systems rely on large synchronous generators (SGs), where the mechanical rotor's inertia naturally stabilizes grid frequency during demand fluctuations. However, the rapid growth of inverter-based renewable energy sources (RES) has transformed modern power systems. Because the inverter-based RES systems lacked the same inertia as normal SG during a disturbance, any sudden changes in frequency and voltage could occur at the point of common coupling (PCC) that reducing system stability. High-RES system penetration will lower system fluctuations and overall power system inertia. The frequency stability of a power grid that primarily uses RES is proposed to be improved by using virtual synchronous generators (VSG). To reduce DC-link voltage fluctuation and stabilize the power system's frequency, VSG with enhanced whale optimization algorithm (WOA) technique for optimizing the PI controller's settings are used in this work. The proposed enhanced WOA integrates chaotic initialization, nonlinear adaptive parameters, elite guidance, and dynamic probability adaptation to ensure faster convergence, prevent premature stagnation, and achieve robust optimization. The system was modeled and simulated in MATLAB/Simulink, where its performance was validated under a scenario of rapid load change. The simulation results demonstrate the benefits of PI tuning with the WOA in 40% reduction in settling time and 65% reduction in system frequency overshoot. Employing the enhanced WOA in the proposed VSG system leads to lower the error rates of the voltage regulator within (800 ±5)V and stabilize the frequency within (50±0.04)Hz of the VSG.

1. INTRODUCTION

In modern microgrids (MG), photovoltaic (PV) systems act as the primary source of clean power. However, the major challenges to maintaining grid stability are the intermittent nature and the lack of inherent inertia. These difficulties are particularly with regard to the regulation of frequency and voltage during dynamic conditions. To overcome such instability, researchers use the Virtual Synchronous Generator (VSG) approach. This VSG control strategy effectively mimics the inertia and damping behavior of traditional synchronous generators. As a result, ensuring smoother and more stable operation [1-3]. The VSG architecture integrates energy storage (batteries or/and supercapacitors), power converters, and control systems to dynamically regulate power flow. It can imitate the electromechanical behavior of synchronous generators [4-6]. The core of the VSG control involves an Enhanced Synchronous Photovoltaic (ESPV) controller that regulates the inverter's active (P) and reactive (Q) power output. Figure (1) illustrates the proposed ESPV controlling as a single-stage grid-connected PV system with energy storage devices and drives. An LCL filter, which filters and reduces harmonic distortion to tolerable levels, connects the load to the inverter output [7, 8].

During grid disturbances, the battery energy storage system (BESS) connected to the DC-link is designed to temporarily inject (in the discharge mode) or absorb (in the charging mode) electricity into the system [9]. A bidirectional buck-boost converter is attached to the BESS to change its input current during charging and discharging. Thus, under typical circumstances, a BESS can be constructed to compensate for a PV system's power intermittency, including variations in solar irradiation or atmospheric conditions [10]. However,

* Corresponding author's E-mail address: mohanadshehab@uomustansiriyah.edu.iq
DOI: 10.24237/djes.2026.19204

the solar plant continues to run in maximum power point tracking (MPPT) mode to attain maximum power efficiency [11, 12].

To regulate voltage and frequency, droop controllers can be implemented in the system. The P-f (active power-frequency) droop controller adjusts the ESPV's phase angle and frequency, while the Q-V (reactive power-voltage) droop controller defines the reference voltage. These controllers rely on active and reactive power as inputs, which are obtained from monitored P-f and Q-V control blocks [13]. For simpler implementation and more robust control, Park's transformation is used. It converts the measured three-phase voltages and currents from the abc system into the dq0 rotating reference frame. Next, a synthesis algorithm merges the phase angle (θ) and reference voltage (Er) to generate the final voltage reference ($V_{dq_{ref}}$) required for regulation. That reference is then fed into the voltage controller to produce the related three-phase reference signals ($V_{abc_{ref}}$) for pulse-width modulation (PWM) [14].

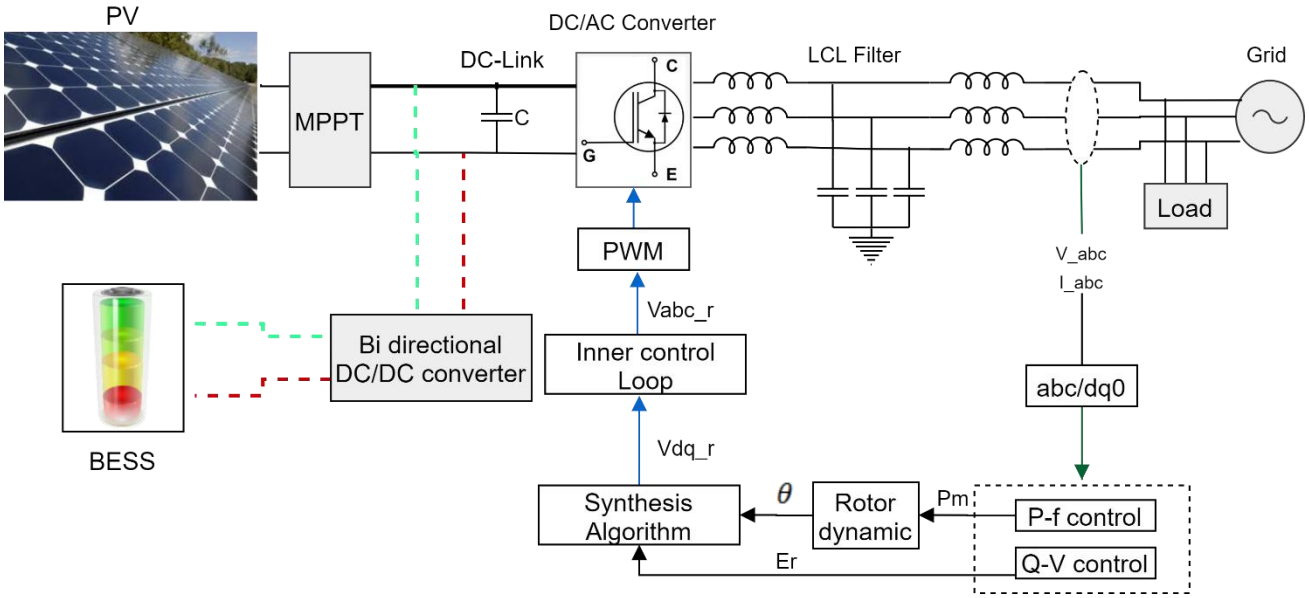

Figure 1. The proposed ESPV/VSG control technique

Conventional PI tuning methods like Ziegler-Nichols, Cohen–Coon, or pole-placement techniques are often ineffective for the complex and non-linear dynamics in PV-VSG systems. They rely on linearized models that cannot covering all problems and require manual fine-tuning which may not achieve the coordinated optimization needed for best frequency stability, voltage regulation, and power quality simultaneously [15, 16]. This gap can be addressed by using a metaheuristic optimization technique like Particle Swarm Optimization (PSO) or Whale Optimization Algorithm (WOA). Our methodology bridges the gap by providing an automated, intelligent tuning process that can find the global optimum PI parameters with ensuring all aspects of the VSG including (frequency, voltage, current) work in harmony for maximum stability and performance.

Several studies such as [17, 18] use simplified system models, fixed network topologies and limited virtual inertia budgets. Such assumptions fail to represent the true nonlinear and coupled dynamics of real-world power systems. Most of these works emphasize frequency stability, paying less attention to voltage regulation, nonlinear effects, and coordinated operation of multiple VSGs.

Although optimization techniques like PSO [19] have been applied, they are often executed offline. As a result, they can face problems such as early convergence, poor adaptability, and an inability to react to real-time disturbances. Additionally, the role of energy storage systems (ESS), transient responses, and practical implementation validation are not fully addressed. As a result, they limit the applicability of these approaches in many objective functions and complex PV-VSG microgrids.

In this study, an enhanced WOA is proposed and applied for coordinated optimization within PV-VSG systems. The proposed WOA incorporates several advanced features with chaotic initialization, adaptive nonlinear parameter adjustment, Lévy flight-based multi-strategy updates, and local search refinement. Together, these modifications improve convergence speed, maintain a balance exploration and exploitation, and enhance overall optimization precision.

This enhanced WOA is employed to determine the optimal PI tuning controller values (K_p and K_i) that are used in conjunction with the voltage regulation and

current controlling. The optimal parameters ensure high-quality power delivery, minimal overshoot, fast settling time, and rapid response to load variations. The remaining sections including the proposed system algorithm design and implementation, simulation results, discussion and the conclusion.

2. THE PROPOSED SYSTEM DESIGN

A bidirectional DC/DC converter is employed to manage the battery charging and discharging. It is implied that the BESS voltage is always lower than the voltage of the DC-link as the boosting topology dictates the design of the DC/DC bidirectional converter [20]. For two-way power conversion, bidirectional dc-dc converters in both boost and buck modes were used. Figure (2) shows the simulation circuit design. The voltage is stepped up (discharge mode) in the boost mode while stepped down (charging mode) in the buck mode.

For the bidirectional DC/DC converter, the inductor (L_B) and resistance (R_B) values are determined by [21]

$$L_B = \frac{D\,(1-D).V_{Bat}}{f_{sw}.\Delta I_C} \quad (1)$$

$$R_B \ll \zeta.\,\mathrm{L_B}.\,\mathrm{f_{sw}} \quad (2)$$

Where D is the duty cycle, f_{sw} is the switching frequency, V_{Bat} is the battery voltage, ΔI_C is the is the inductor's ripple current, and ζ is the damping factor. The control system must coordinate both of the DC/DC converter switches S_1 and S_2. The inner current loop controls the battery's current in order to continuously monitor the i_{Bat}^{**}. The outer voltage loop creates a reference signal for the inner loop i_{Bat}^{*} and hence, regulates the DC-link voltage.

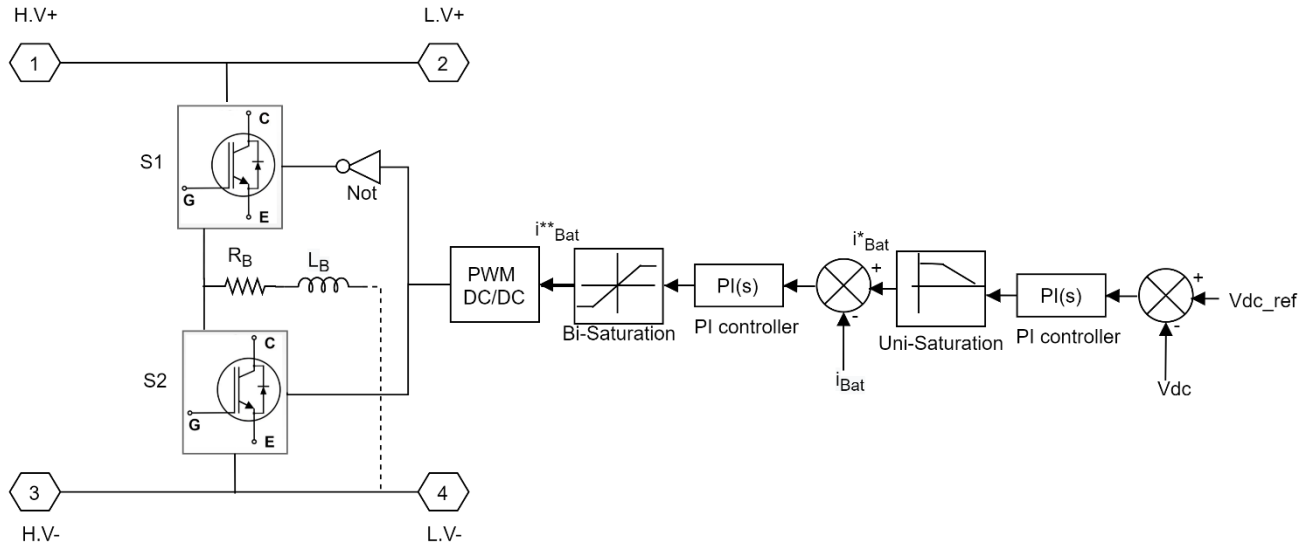

Figure 2. Bidirectional DC/DC converter Simulink diagram

The power system has to be sure that the voltage remains within the permitted fluctuation range while it is operating normally. To maintain the stability of the power system voltage, a dynamic balance between the generated and the consumed P&Q powers in respect to the operational voltages and their frequency is required. The rotor dynamics block of SGs links frequency to the balance between generation and load. When frequency drops, increasing active power injection can mimic inertia, reducing generation and/or load imbalances. PV systems as shown in Figure (3) can similarly support the grid by providing virtual inertia, helping maintain stable operation during disturbances. The P, Q, V, and f-parameters of the system in Figure (4) are controlled, which is necessary to stabilize the operation of the suggested system.

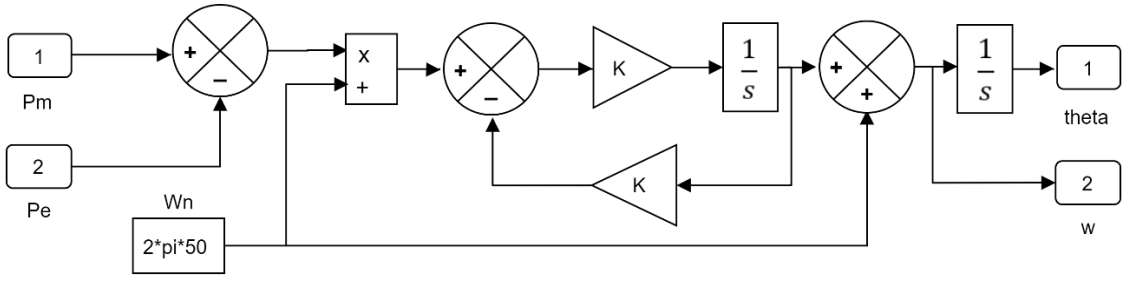

Figure 3. The rotor dynamics block Simulink implementation

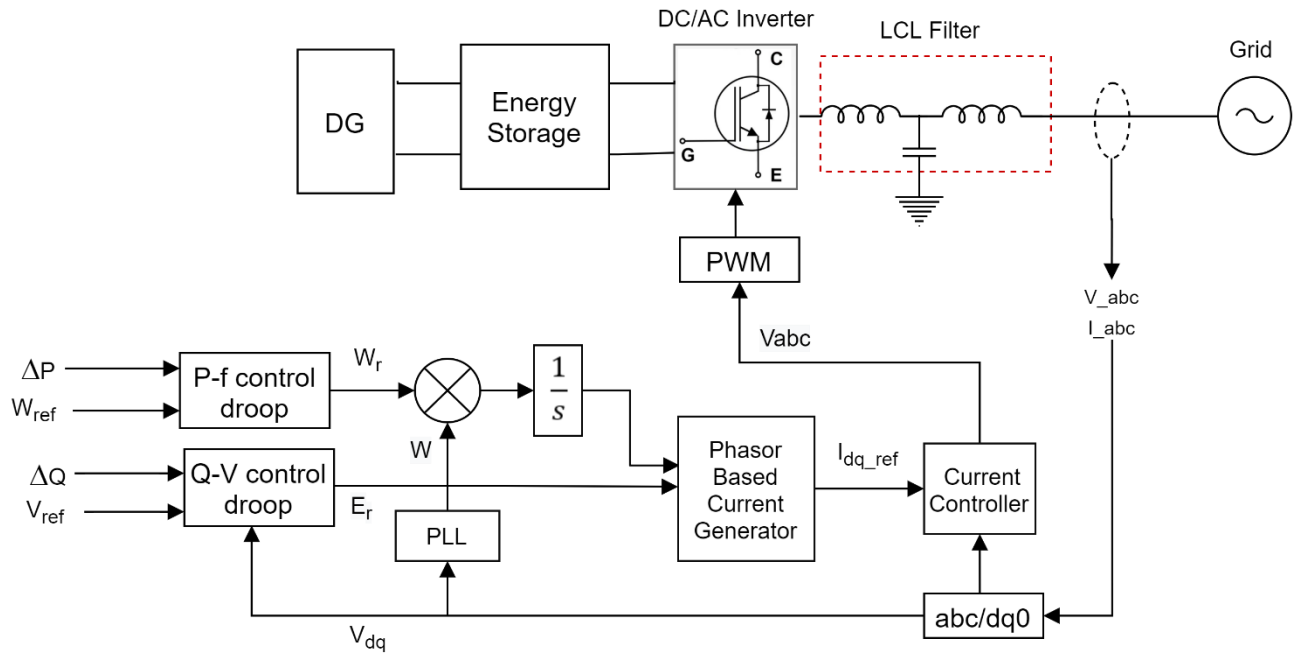

Figure 4. The proposed system with the regulation of P, Q, V, f-parameters

The synchronous generator (SG) is the main source of reactive power (Q) in the power system. The system's reactive power balance is maintained by the excitation regulator's management of its reactive power output, which guarantees an appropriate distribution of system reactive power among parallel-operating generator sets [22]. Similarly, active power sharing between generators is controlled by the real power-frequency (P-f) characteristic, where a droop control mechanism maintains stability by adjusting the output power in response to frequency fluctuations. Frequency variations show imbalances between generation and demand, whereas the system voltage fluctuates with the load during normal operation.

In order for the VSG to simulate the excitation control function of an SG and guarantee equitable reactive power distribution and system voltage stability, the reactive power-voltage (Q-V) controller was created [23]. Similarly, the active power-frequency (P-f) regulation of the VSG helps to preserve frequency stability under load variations by simulating the droop and inertial response of conventional SGs. Figure (5) displays the frequency-real power characteristic curve and the corresponding Simulink block diagram, which show how power output and grid frequency are dynamically related.$P_n = P_{ref} - k_p(f_{ref} - f_n)$ and hence

$$k_p = \frac{P_{ref} - P_n}{f_{ref} - f_n} = \frac{\Delta P}{\Delta f} \quad (3)$$

With the same idea, the voltage-reactive power characteristic curve and equivalent Simulink block diagram are shown in Figure (6).

$V_{ref} = V_r = V_n + k_{v\,(}Q_n - Q_r)$ and hence

$$k_v = -\frac{V_r - V_n}{Q_r - Q_n} = -\frac{\Delta V}{\Delta Q} \quad (4)$$

where k_v is the voltage regulation factor, ΔV is the fluctuation in SG output voltage, and ΔQ is the change in SG reactive electrical power. V_r and Q_r are the rated SG produced voltage and reactive power. V_n and Q_n are the expected voltage and reactive power values of the generator. Finally, E_r represents the excitation voltage amplitude in the VSG control scheme.

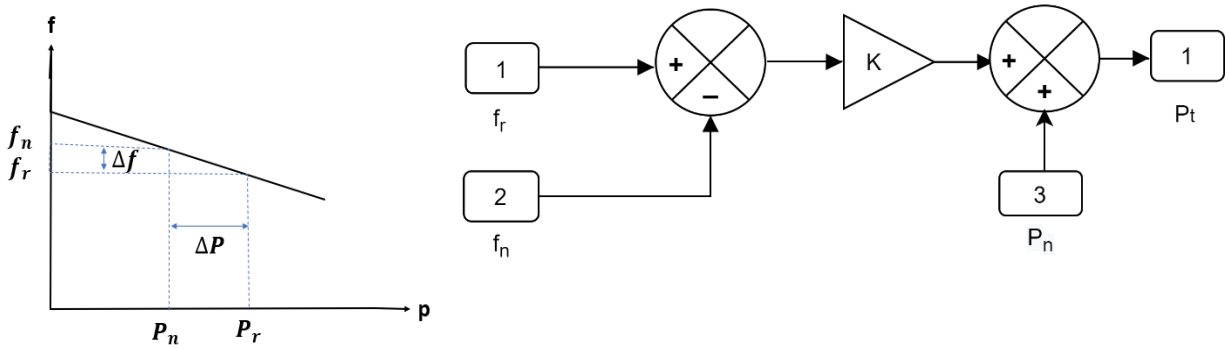

Figure 5. Frequency-Real power control with schematic diagram

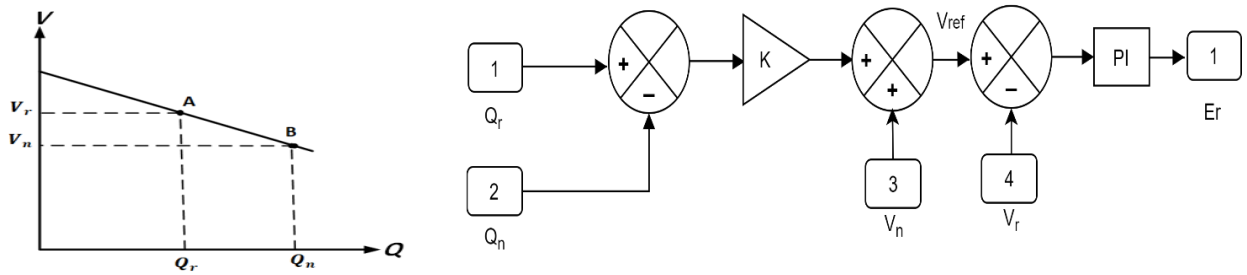

Figure 6. Voltage-Reactive power control with schematic diagram

3. PI-BASED WOA ALGORITHM

For load settings, the PI controller frequently relies on a linear system equation. Its popularity in inverter systems stems from its high reliability, simple design, and effective control coordination. In AC systems, the PI controller is commonly employed for regulating grid current and DC-link voltage, making it a standard choice for most voltage and current control applications. The inverter's DC-link voltage remains steady, and the power that is pumped into the grid is appropriately managed. Even while PI controllers are usually easy to adjust, reaching an ideal and totally reliable solution is made extremely difficult by nonlinear load fluctuations and system disruptions [24, 25]. To minimize transient response, reduce overshoot, and achieve low steady-state error under load demand alterations, the WOA method is utilized to find the optimal values of K_p and K_i and hence lower error for the voltage regulator and current controller.

4. WOA ALGORITHM IMPLEMENTATION

Alsalibi et al. [26] presented the Whale optimization Algorithm (WOA), a metaheuristic optimization method that draws inspiration from the distinctive foraging habits of humpback whales. They are remarkably intelligent because these marine creatures' brains include spindle cells that are identical to those in humans [27]. The biological basis for WOA's optimization mechanism is their unique bubble-net hunting technique, in which they use spiraling bubble structures to trap prey [28]. Encircling prey, bubble-net attacking (exploitation), and random search (exploration) are the three main stages of WOA. The periods are mathematically simulated according to the whales 'upward-spirals' and 'double-loops' motions that is based on [29] research. WOA is now widely used in engineering applications, such as:

1. Tuning PI Controllers: Optimizing proportional-integral (PI) parameters (K_p and K_i) for improved dynamic response in grid-tied inverters [30,31], because of its ability to strike a balance between exploration and exploitation. It operates offline to determine fixed PI controller gains which are then applied during real-time simulation.
2. Enhancing active power-frequency (P-f) and reactive power-voltage (Q-V) droop controls: emulating SG behavior in renewable-integrated grids as in the VSGs [32].
3. Partial shadowing of photovoltaic (PV) systems: Optimizing and hence reaching to the power point tracking (MPPT) [33].

Recent research shows that WOA outperforms classical techniques in improving stability, reducing overshoot, and accelerating convergence for VSG-based microgrids [34]. The enhanced WOA algorithm further improves overall performance through chaotic initialization that leads to faster convergence. In addition, nonlinear parameter adaptation to prevent premature convergence. And finally, an elite guidance mechanism that directs the search toward more promising regions. Additionally, dynamic probability adaptation helps balance exploration and exploitation throughout the optimization process. The following presents the pseudo-code of the improved WOA algorithm for optimal PI tuning.

Pseudo-code: Enhanced WOA algorithm for Kp & Ki tuning

1. Initialization:
- Define PI, i.e., Kp (proportional gain), Ki (integral gain) parameters to be optimized
- Set EWOA parameters:
  Population size (n), max iterations (tmax)
  Search space bounds: Kp ∈ [Kp_{min}, Kp_{max}], Ki ∈ [Ki_{min}, Ki_{max}]

2. Chaotic Initialization (using Logistic Map):
- Set algorithmic constants:

Chaos coefficient (c=4.0), adaptive weight (w), Lévy flight parameter (β=1.5), step-size factors (α = 0.6, γ = 0.1).
- Generate initial population using Logistic map:

$x_{next} = c \times x_{current} \times (1 - x_{current})$
- Randomly initialize each whale position:

Each whale Xi = [Kp_i, Ki_i] for i = 1,...,n
- Define the objective function f(Xi) (overshoot, settling time, absolute error)
- Evaluate initial fitness for all whale
- Identify the current best whale Xbest = [Kp, Ki]

3. Optimization Loop (while t < tmax):

a. For each whale Xi = [Kp_i, Ki_i]:

i. Update WOA coefficients:

- a = 2 × (1 - t/tmax) // Exploration-exploitation balance
- A = 2a × rand( ) - a // Random vector
- C = 2 × rand( ) // Random vector
- p = rand( ) // Behavior selection probability

ii. Update whale position:

- If (p < 0.5):
  - If (|A| < 1): // Local search around best PI

D = |C ⊙ X - Xi| // ⊙: element-wise multiplication

Xi_new = X - A ⊙ D

  - Else: // Global search

Select random whale X_rand

D = |C ⊙ X_rand - Xi|

Xi_new = X_rand - A ⊙ D

- Else (p ≥ 0.5): // Spiral search

D = |Xbest - Xi|

Xi_new = D ⊙ $e^{(bl)}$ ⊙ cos(2πl) + Xbest // b: spiral shape constant

iii. Apply PI constraints:

- Apply Kp_i ∈ [Kp_{min}, Kp_{max}]
- Apply Ki_i ∈ [Ki_{min}, Ki_{max}]

iv. Evaluate new candidate:

- Simulate system with [Kp_i, Ki_i]
- Calculate fitness f(Xi_new) using:

f = α×overshoot + β×settling time + γ×absolute error // Weighted objective

v. Update position if improved:

- If f(Xi_new) < f(Xi), set Xi = Xi_new

b. Update the best solution:

- Xbest = whale with minimum f(Xi) in population

c. Increment iteration:

- t = t + 1

4. Termination:

- Return optimal PI gains [Kp, Ki]
- Implement these gains in the PV-VSG control system

5. RESULTS

A 0.25MW PV system feeds into the grid. Table (1) lists the simulated ESPV/VSG parameters. Under large disturbances, the ESPV can exceed stability limits, risking frequency deviation and system failure. The VSG ensures stability under these conditions. Figure (7) illustrates the PV's voltage, current, and power curves. The PV system initially supplies a 0.25MW local load under normal and standard test conditions (daylight temperature is 25°, and solar radiation is 1000 W/m^2).

Table 1: The established setup parameters

Parameters	Values	Parameters	Values
DC voltage	~800 V	Bidirectional inductor (L_B)	0.2 mH
Line Grid AC voltage	380 V	Bidirectional resistance (R_B)	0.06 Ω
Rated power	¼ MW	Filter inductor (L_f)	0.5 mH
Rated frequency	50 Hz	Filter capacitor (C_f)	60 µF
Switching frequency	10 kHz	K_v, K_p droop coefficients	1e-3 to 1e-4

As seen in Figure (8), the load experiences a 20% step increase to 300 kW at time t = 1 sec, followed by a return to the nominal 250 kW load at t = 2 sec. As illustrated in Figure (9), the ESPV/VSG system generates stable output voltage and current waveforms under the specified operating conditions. A resistive local load tests the P-f controller's performance under real power fluctuations. With 100 kVAR reactive power, 1000 W/m^2 irradiance, and 25°C, the PV system shares the load with the grid and VSG. Figure (10) shows the dynamic response to load changes: real power steps from 300 kW to 350 kW at t = 1s, then back to 300 kW at t = 2s.

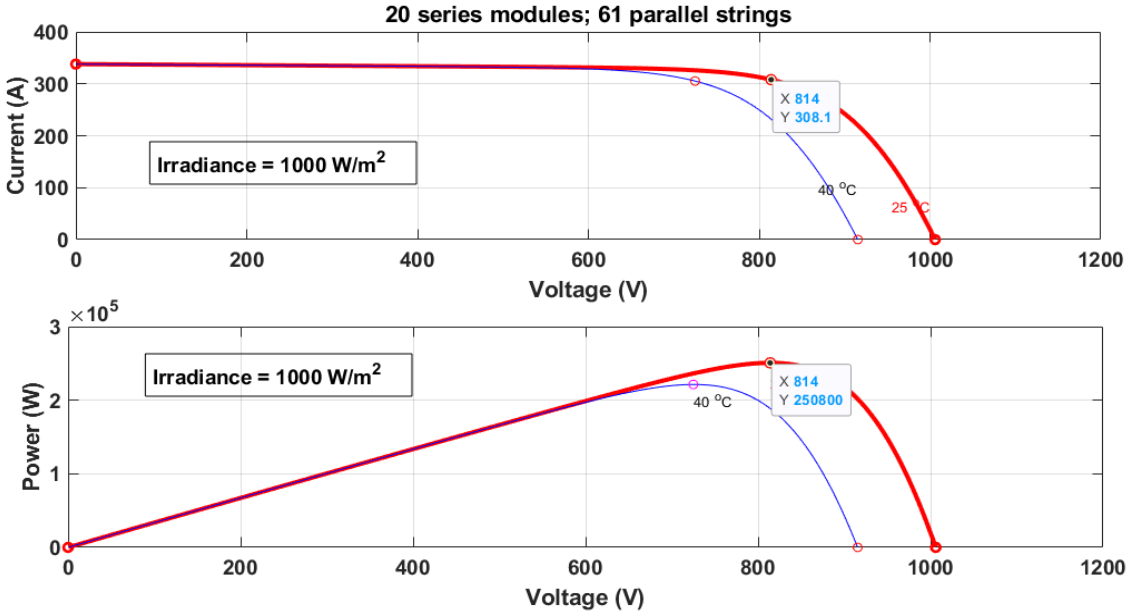

Figure 7. The current-voltage and power-voltage curves of the utilized PV array

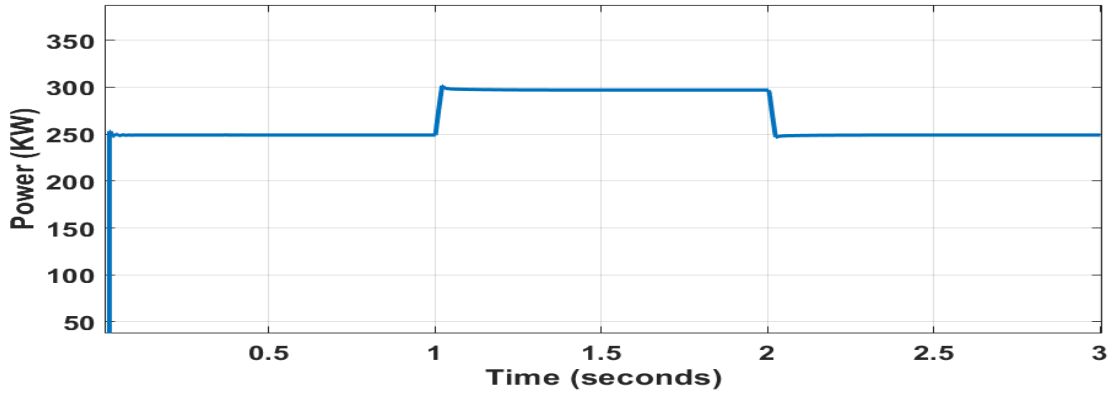

Figure 8. Active power waveform due to the sudden variation of the load

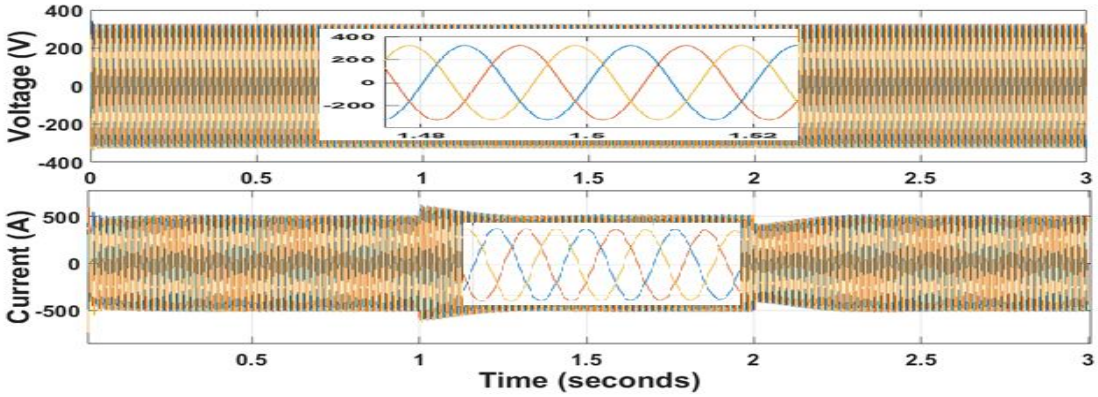

Figure 9. The resulting voltage and current of the ESPV/VSG with the real power change

The VSG's Q-V control was tested by varying the reactive power load. Initially, the system operates at 100 kVAR reactive power and 300 kW active power, with PV conditions of 25°C and 1000 W/m^2 irradiance. An inductive load steps the reactive power by +50 kVAR at t = 1s and returns at t = 2s, while active power remains fixed at 300 kW. System parameters match those used in active power tests. Simulation results are shown in Figure (11).

Figure (12) shows the immediate impact on bus voltage, which dropped from 229 Vrms to 227 Vrms when the reactive load increased by 50 kVAR at t = 2s, where the resultant droop voltage is 1.3V. The whole system voltages responses including DC-bus link and PV output voltages is detailed in Figure (13).

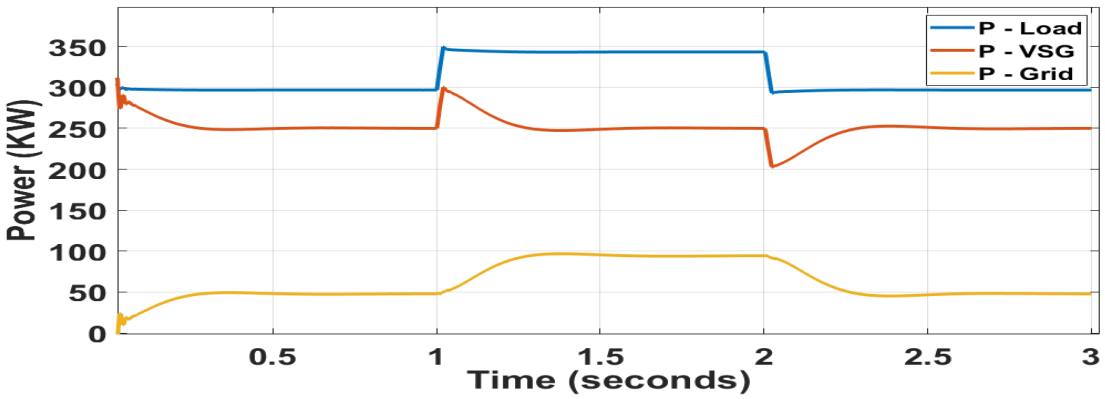

(a)

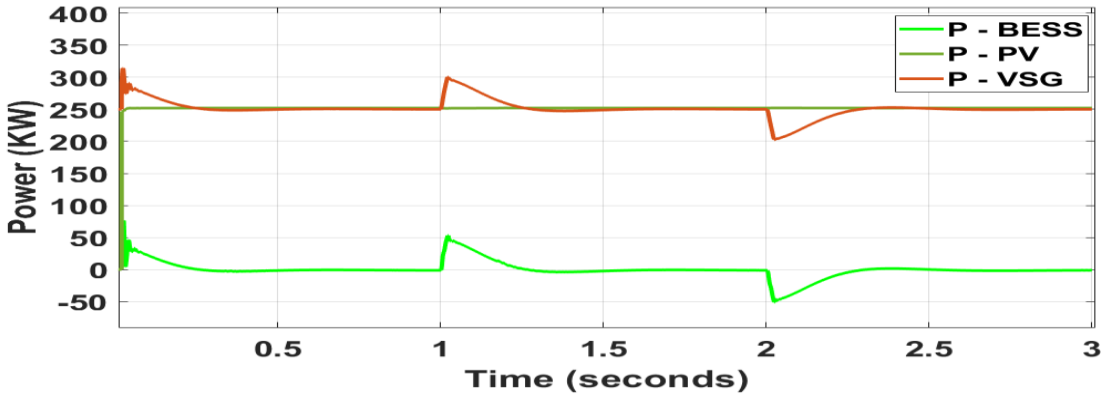

(b)

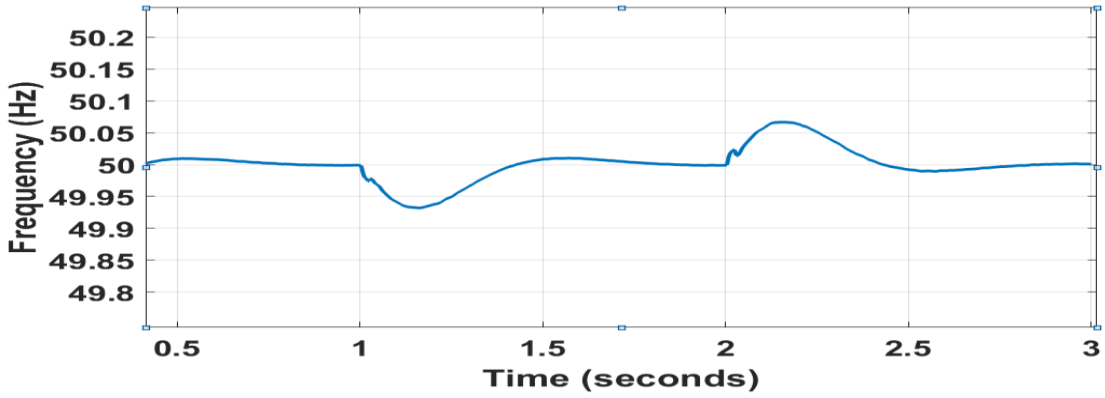

(c)

Figure 10. Dynamic reaction of the system to changes in real power (a) Active power of the system (b) Active power of the VSG output (c) System frequency waveform

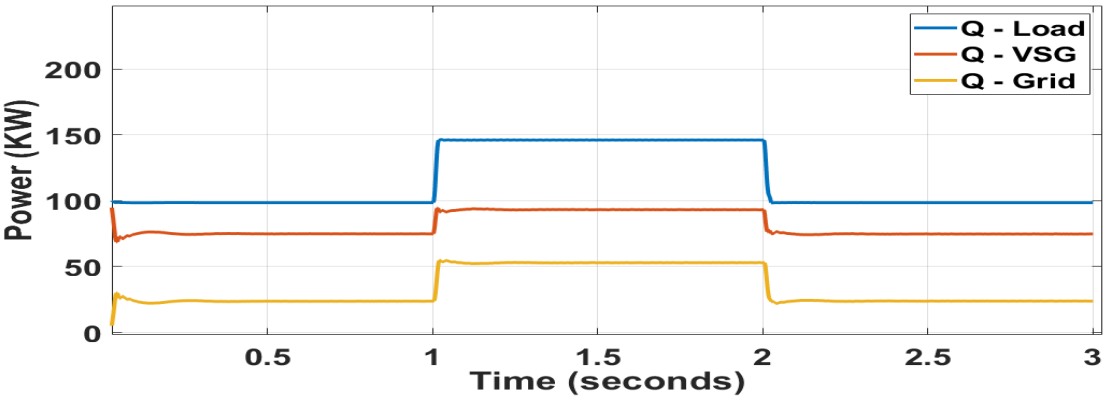

Figure 11. The system's reactive electrical power reaction to a change in actual power

Figure 12. The bus voltages response to a change in reactive power

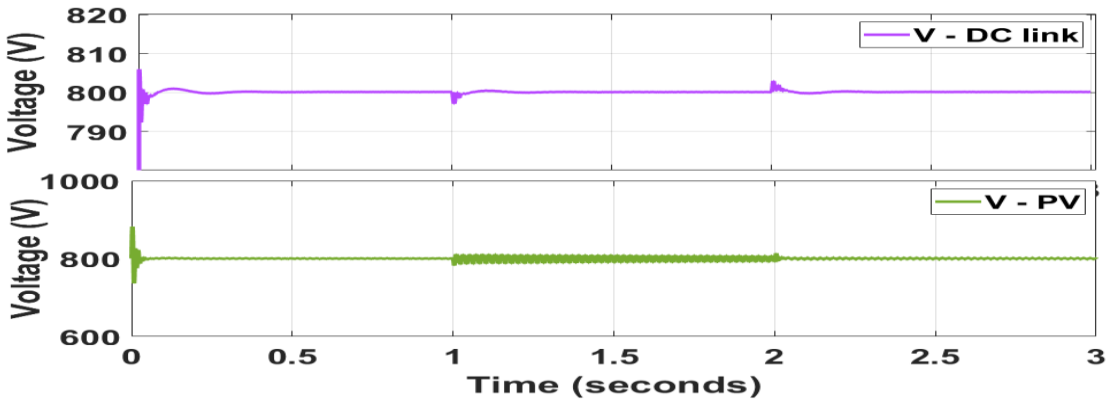

Figure 13. The system's voltages responses including for both DC-bus link and PV output

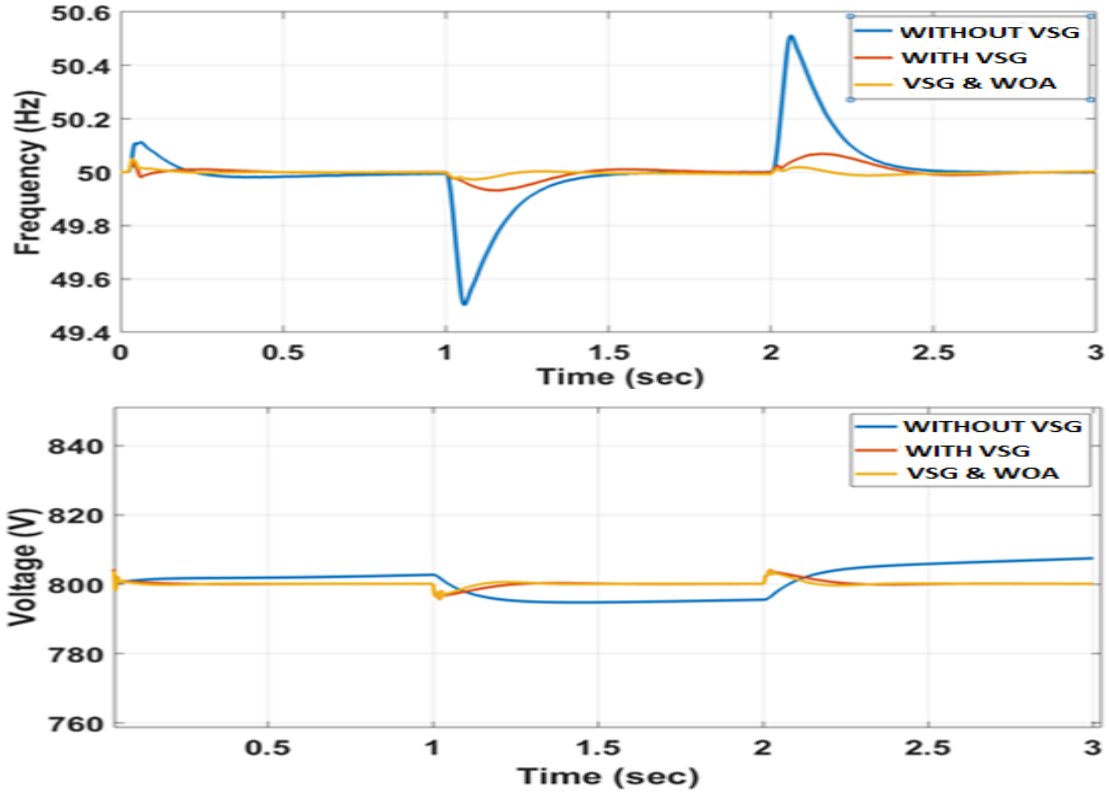

Figure 14. System frequency and voltage responses under various operation cases

A grid-connected PV system is assessed using a VSG model that provides energy to the load in order to examine its properties in regards to adjusting its output in response to variations in the load, where the WOA is used to optimize the VSG controller settings. The system frequency and DC link voltage without VSG,

PV with VSG, and VSG-WOA are indicated in Figure (14). It illustrates how the system frequency for PV without VSG fluctuates sharply and quickly in response to abrupt changes in load. Furthermore, a quick change in the load causes the DC-link voltage to fluctuate significantly. Particularly, when VSG is attached to the WOA, the system's voltage fluctuation drops substantially within acceptable limits, and the frequency transfer is steadier and with low change.

To test the voltage and frequency fluctuations under different PV generations and load varying conditions scenarios. The proposed methods are examined with varying solar irradiance intensity that is swinged between 1000 W/m^2 - 500 W/m^2 of solar radiation with a solar temperature of 25° under high and moderate load abrupt changes, i.e., with the load is quickly raised by 100 kW or raised by 50 kW. At time t= 0.03s, the irradiance = 1000 W/m^2 with high load abrupt change. Then, at time t= 0.5s the irradiance becomes 500 W/m^2 with the same high load change. After that, at time t= 1s, the irradiance returns to 1000 W/m^2 with moderate load sudden change. Finally, at time t=1.5s, the irradiance is changed to 500 W/m^2 under the same moderate load effect.

Figures (15 - 16) show the frequency variation and corresponding DC-voltage of this scenario. They approve the superiority of the VSG-WOA steady and transit responses over other traditional and VSG-PSO approaches in achieving lower frequency and voltage overshoots with low settling times.

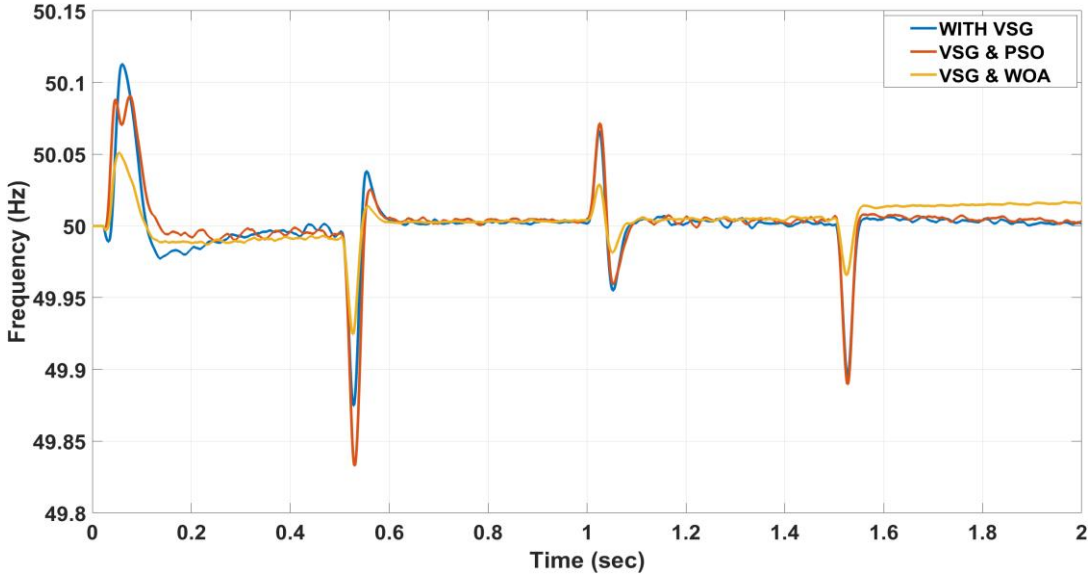

Figure 15. Frequency variation with 1000 W/m^2 - 500 W/m^2 irradiation and load change

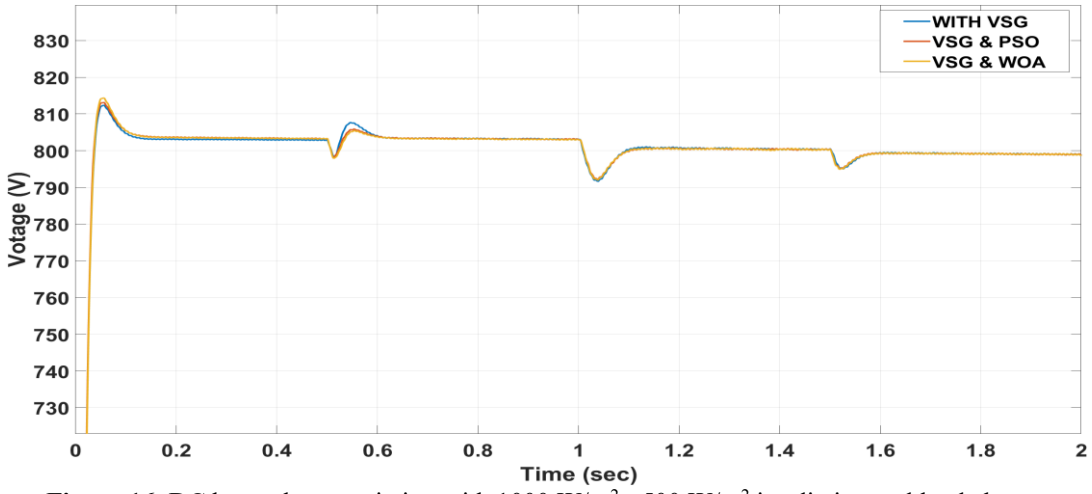

Figure 16. DC bus voltage variation with 1000 W/m^2 - 500 W/m^2 irradiation and load change

6. DISCUSSION

The DC-link voltage is not constant and fluctuates significantly with a sudden change in load. Additionally, Figures (10) and (14) demonstrate how quickly and steeply the system frequency for PV without VSG fluctuates in response to a sudden change in load. The frequency change rate is higher than what is permitted. Therefore, slight variations in frequency

and voltage could negatively impact the stability of the system. The system's frequency and rate fluctuate very little within allowed limits when VSG is connected, and the frequency and rate change more slowly and gradually. This is due to the fact that the battery system banks inject energy when the load increases and absorb electricity by charging themselves for a short time when the demand decreases until the grid provides power to the load or receives additional power from the PV.

Because the DC link voltage using the VSG and WOA techniques responds faster than without the VSG approach in stabilizing the DC input voltage for the inverter system, the results as seen in Table (2) show that the rising times of the VSG and WOA are comparable and shorter than those of the VSG-free (without optimization) method. Furthermore, compared to the VSG approach alone, the PI controller using the VSG/WOA techniques has returned to the steady-state condition more quickly. Table (2) also illustrate the outperforming of the VSG/WOA over VSG/PSO [19] in lowering the maximum peak overshoot (MP) and steady state or settling time (Ts). The VSG/WOA optimized parameters enable the system to respond more quickly and in higher steady DC input to the inverter that can providing the required power during a sudden change in load.

Table 2: The DC-link and frequency variation performances under load changes

The Proposed VSG/WOA				The VSG/PSO [19]			
Technique	**Frequency peak to peak (Hz)**	**Voltage overshoot (%)**	**Settling time (s)**	**Technique**	**Frequency peak to peak (Hz)**	**Voltage overshoot (%)**	**Settling time (s)**
Without VSG	0.96	1.125	0.228	Without VSG	0.86	-	0. 739
VSG	0.246	0.625	0.136	VSG	0.384	-	0. 611
VSG-WOA	0.103	0.437	0.106	VSG-PSO	0.1304	-	0. 289

ACKNOWLEDGMENT

The authors would like to thank the Mustansiriyah University (www.uomustansiriyah.edu.iq), Baghdad-Iraq for its support in the present work.

7. CONCLUSION

This study presented a robust control approach designed to enhance the dynamic stability of renewable energy-based power systems through integrating the Virtual Synchronous Generator (VSG) with an enhanced Whale Optimization Algorithm (WOA). It made the system keep stable steady state and transient operations under varying load conditions. The proposed method successfully balanced simplicity and adaptability with ensuring reliable frequency and voltage regulation even during demanding scenarios. The enhanced WOA played a central role in optimizing the proportional–integral (PI) controller parameters of the VSG via employing mechanisms such as chaotic initialization, nonlinear adaptive tuning, elite guidance, and dynamic probability adaptation. the algorithm achieved faster convergence with avoiding early stagnation, and hence enhanced control precision. These improvements contributed to smoother and enhance performance across a wide range of operating conditions.

Simulation studies conducted in MATLAB/Simulink (Version 2023b) confirming the effectiveness of the proposed strategy. Under sudden and rapid load variations, the WOA-optimized PI controller consistently outperformed conventional and PSO tuning methods. It achieved a 65% reduction in frequency overshoot, a 6% reduction in voltage overshoot, and a 40% decrease in settling time. Moreover, voltage and frequency remained within their safe operating limits: (800 ± 5) V and (50 ± 0.04) Hz, respectively.

In conclusion, pairing VSG with the advanced WOA gives the grid a dependable and steady supply of voltage and current. Future research will aim to extend this work by incorporating adaptive machine learning based control for real time parameter tuning and by validating the approach through hardware-in-the-loop (HIL) experiments under realistic grid environments.

REFERENCES

[1] W. Sang, W. Guo, S. Dai, C. Tian, S. Yu, and Y. Teng, "Virtual synchronous generator, a comprehensive overview," Energies, vol. 15, no. 17, p. 6148, 2022. doi: 10.3390/en15176148.

[2] V. Thomas, S. Kumaravel, and S. Ashok, "Reduction of frequency oscillations in solar PV microgrid using virtual synchronous machine," in Proc. Int. Conf. Power Electron. Appl. Technol. Present Energy Scenario (PETPES), 2019, pp. 1–5. doi: 10.1109/PETPES47060.2019.9003957.

[3] U. Bose, S. K. Chattopadhyay, C. Chakraborty, and B. Pal, "A novel method of frequency regulation in microgrid," IEEE Trans. Ind. Appl., vol. 55, no. 1, pp. 111–121, 2019. doi: 10.1109/TIA.2018.2866321.

[4] A. Belila, Y. Amirat, M. Benbouzid, E. Berkouk, and G. Yao, "Virtual synchronous generators for voltage synchronization of a hybrid PV-diesel power system," Int. J. Electr. Power Energy Syst., vol. 117, May 2020, Art. no. 105707. doi: 10.1016/j.ijepes.2019.105707.

[5] M. M. Badreldien and B. K. Johnson, "Virtual synchronous generator controller for solar photovoltaic system," in Proc. IEEE Electr. Power Energy Conf. (EPEC), Oct. 2021, pp. 480–485. doi: 10.1109/EPEC52095.2021.9621570.

[6] H. Ur Rehman, X. Yan, M. A. Abdelbaky, M. Ullah Jan, and S. Iqbal, "An advanced virtual synchronous generator control technique for frequency regulation of grid-connected PV system," Int. J. Electr. Power Energy Syst., vol. 125, 2021, Art. no. 106440. doi: 10.1016/j.ijepes.2020.106440.

[7] T. Muthamizhan, M. J. Kumar, P. Rathnavel, M. Aijaz, and A. Sivakumar, "A photovoltaic fed high gain bidirectional DC/DC converter on EV charging stations applications," in Proc. 2nd Global

Conf. Advancement Technol. (GCAT), Oct. 2021, pp. 1–6. doi: 10.1109/GCAT52182.2021.9587664.
[8] P. Bhuvela, H. Taghavi, and A. Nasiri, "Design methodology for a medium voltage single stage LLC resonant solar PV inverter," in Proc. 12th Int. Conf. Renewable Energy Res. Appl. (ICRERA), Aug. 2023, pp. 556–562. doi: 10.1109/ICRERA59003.2023.10269330.
[9] D. Borkowski, P. Oramus, and M. Brzezinka, "Battery energy storage system for grid-connected photovoltaic farm–Energy management strategy and sizing optimization algorithm," J. Energy Storage, vol. 72, 2023, Art. no. 108201. doi: 10.1016/j.est.2023.108201.
[10] C. Zhao, P. B. Andersen, C. Træholt, and S. Hashemi, "Grid-connected battery energy storage system: a review on application and integration," Renew. Sustain. Energy Rev., vol. 182, 2023, Art. no. 113400. doi: 10.1016/j.rser.2023.113400.
[11] M. L. Katche, A. B. Makokha, S. O. Zachary, and M. S. Adaramola, "A comprehensive review of maximum power point tracking (MPPT) techniques used in solar PV systems," Energies, vol. 16, no. 5, p. 2206, 2023. doi: 10.3390/en16052206.
[12] B. Hamid, I. Hussain, S. J. Iqbal, B. Singh, S. Das, and N. Kumar, "Optimal MPPT and BES control for grid-tied DFIG-based wind energy conversion system," IEEE Trans. Ind. Appl., vol. 58, no. 6, pp. 7966–7977, 2022. doi: 10.1109/TIA.2022.3192689.
[13] S. M. Azizi, "Robust controller synthesis and analysis in inverter-dominant droop-controlled islanded microgrids," IEEE/CAA J. Autom. Sinica, vol. 8, no. 8, pp. 1401–1415, 2021. doi: 10.1109/JAS.2021.1004009.
[14] P. A. Gbadega and O. A. Balogun, "Active and reactive power droop controller design for reliable and optimal control of renewable-based micro-grid," Adv. Eng. Forum, vol. 41, pp. 111–136, Aug. 2021. doi: 10.4028/www.scientific.net/AEF.41.111.
[15] M. C. Rais, F. Z. Dekhandji, A. Recioui, M. S. Rechid, and L. Djedi, "Comparative study of optimization techniques based pid tuning for automatic voltage regulator system," Eng. Proc., vol. 14, no. 1, p. 21, 2022. doi: 10.3390/engproc2022014021.
[16] Y. O. M. Sekyere, P. O. Ajiboye, F. B. Effah, and B. T. Opoku, "Optimizing PID control for automatic voltage regulators using ADIWACO PSO," Sci. Afr., vol. 27, 2025, Art. no. e02562. doi: 10.1016/j.sciaf.2024.e02562.
[17] W. J. Farmer and A. J. Rix, "Optimising power system frequency stability using virtual inertia from inverter-based renewable energy generation," IET Renew. Power Gener., vol. 14, no. 15, pp. 2820–2829, 2020. doi: 10.1049/iet-rpg.2020.0351.
[18] B. Pournazarian, R. Sangrody, M. Saeedian, M. Lehtonen, and E. Pouresmaeil, "Simultaneous optimization of virtual synchronous generators (VSG) parameters in islanded microgrids supplying induction motors," IEEE Access, vol. 9, pp. 124972–124985, 2021. doi: 10.1109/ACCESS.2021.3110668.
[19] R. F. Idan, A. J. Mahdi, and T. M. A. Wahhab, "Optimized proportional-integral controller for a photovoltaic-virtual synchronous generator system," Int. J. Power Electron. Drive Syst. (IJPEDS), vol. 13, no. 1, pp. 509–519, 2022. doi: 10.11591/ijpeds.v13.i1.pp509-519.
[20] C. Zhong, H. Li, Y. Zhou, Y. Lv, J. Chen, and Y. Li, "Virtual synchronous generator of PV generation without energy storage for frequency support in autonomous microgrid," Int. J. Electr. Power Energy Syst., vol. 134, 2022, Art. no. 107343. doi: 10.1016/j.ijepes.2021.107343.
[21] J. Zeng, X. Du, and Z. Yang, "A multiport bidirectional DC–DC converter for hybrid renewable energy system integration," IEEE Trans. Power Electron., vol. 36, no. 11, pp. 12281–12291, 2021. doi: 10.1109/TPEL.2021.3075471.
[22] X. Xiong, C. Wu, and F. Blaabjerg, "An improved synchronization stability method of virtual synchronous generators based on frequency feedforward on reactive power control loop," IEEE Trans. Power Electron., vol. 36, no. 8, pp. 9136–9148, 2021. doi: 10.1109/TPEL.2021.3052163.
[23] S. K. Behera, A. K. Panda, and N. V. Naik, "Adaptive active and reactive power control strategy for virtual synchronous generator," Int. J. Circ. Theor. Appl., vol. 52, no. 6, pp. 2635–2654, 2024. doi: 10.1002/cta.3875.
[24] J. Zhang, T. Zhang, G. Zhang, and M. Kong, "Parameter optimization of PID controller based on an enhanced whale optimization algorithm for AVR system," Oper. Res., vol. 23, no. 3, p. 44, 2023. doi: 10.1007/s12351-023-00781-x.
[25] X. Yang and J. Guan, "PI parameters tuning for frequency tracking control of wireless power transfer system based on improved whale optimization algorithm," IEEE Access, vol. 12, pp. 13055–13069, 2024. doi: 10.1109/ACCESS.2024.3354781.
[26] B. Alsalibi, S. Mirjalili, L. Abualigah, R. I. Yahya, and A. H. Gandomi, "A comprehensive survey on the recent variants and applications of membrane-inspired evolutionary algorithms," Arch. Comput. Methods Eng., vol. 29, pp. 3801–3817, 2022. doi: 10.1007/s11831-022-09721-0.
[27] P. R. Hof and E. Van der Gucht, "Structure of the cerebral cortex of the humpback whale, Megaptera novaeangliae (Cetacea, Mysticeti, Balaenopteridae)," Anat. Rec., vol. 290, no. 1, pp. 1–31, 2007. doi: 10.1002/ar.20407.
[28] S. Mirjalili and A. Lewis, "The whale optimization algorithm," Adv. Eng. Softw., vol. 95, pp. 51–67, 2016. doi: 10.1016/j.advengsoft.2016.01.008.
[29] D. Wiley, C. Ware, A. Bocconcelli, D. Cholewiak, A. Friedlaender, M. Thompson, and M. Weinrich, "Underwater components of humpback whale bubble-net feeding behaviour," Behaviour, vol. 148, no. 5-6, pp. 575–602, 2011. doi: 10.1163/000579511X570893.
[30] K. S. Simhadri and B. Mohanty, "Performance analysis of dual-mode PI controller using quasi-oppositional whale optimization algorithm for load frequency control," Int. Trans. Electr. Energy Syst., vol. 30, no. 1, 2020, Art. no. e12159. doi: 10.1002/2050-7038.12159.
[31] Y. Qun and H. Jie, "Application of WOA-RBF-PI controller in voltage control of SVC," in Proc. IEEE 6th Int. Electr. Energy Conf. (CIEEC), May 2023, pp. 644–649. doi: 10.1109/CIEEC58067.2023.10166259.
[32] L. Tan, M. Yi, L. Cai, H. Zhang, P. Hou, and J. Han, "Adaptive control strategies for improving frequency response parameters in VSG," IEEE Access, vol. 12, pp. 75649–75660, 2024. doi: 10.1109/ACCESS.2024.3407835.
[33] M. Premkumar and R. Sumithira, "Humpback whale assisted hybrid maximum power point tracking algorithm for partially shaded solar photovoltaic systems," J. Power Electron., vol. 18, no. 6, pp. 1805–1818, 2018. doi: 10.6113/JPE.2018.18.6.1805.
[34] T. Liu, S. Liu, H. Yu, Z. Wu, J. Tong, and Q. Yuan, "Research on hybrid approach for maximum power point tracking of photovoltaic systems under various operating conditions," Electronics, vol. 13, no. 19, p. 3880, 2024. doi: 10.3390/electronics13193880.